energies

Article

Application of Alternating Current Stress Measurement Method in the Stress Detection of Long-Distance Oil Pipelines

Jinyao Duan [1], Kai Song [1,*], Wenyu Xie [1], Guangming Jia [2] and Chuang Shen [1]

[1] School of Testing and Optoelectronic Engineering, Nanchang Hangkong University, Nanchang 330063, China; duanjinyaoa@163.com (J.D.); qq1002389603@163.com (W.X.); sw20120329@163.com (C.S.)
[2] PipeChina North Pipeline Company, Langfang 065000, China; jiagm@pipechina.com.cn
* Correspondence: songkai@nchu.edu.cn

Abstract: With the development of pipeline networks, many safety accidents were caused by pipeline stress concentration; it is of great significance to accurately monitor the pipeline stress state for maintaining pipeline safety. In this paper, based on alternating current stress measurement (ACSM) methods, a 3D simulation model of a pipeline electromagnetic field was established by ANSYS software. The distribution law of the pipeline magnetic field and eddy current field were analyzed, and the influence of size and structure parameters of the coil inside the probe were studied. The internal stress detection system of the pipeline was designed, and the static tensile stress measurement experiment was carried out. Simulation and test results showed that the excitation coil with a larger diameter-to-height ratio had a higher measurement sensitivity. The sensitivity of the probe decreased monotonically with the increase of the difference between inner diameter and outer diameter of the detection coil. It increased monotonically with the increase of the equivalent radius of the detection coil. The best measurement results were obtained when the detection coil was located at the center of the two legs of the U-magnetic core. The results showed that the system could identify the pipeline stress concentration area effectively after detection engineering.

Keywords: alternating current stress measurement; pipe stress; electromagnetic field simulation; long-distance oil pipeline inspection

check for updates

Citation: Duan, J.; Song, K.; Xie, W.; Jia, G.; Shen, C. Application of Alternating Current Stress Measurement Method in the Stress Detection of Long-Distance Oil Pipelines. *Energies* **2022**, *15*, 4965. https://doi.org/10.3390/en15144965

Academic Editors: Songling Huang, Xiaochun Song and Lisha Peng

Received: 6 June 2022
Accepted: 1 July 2022
Published: 6 July 2022

1. Introduction

Pipeline transportation has been widely used in oil and natural gas and other important energy-transportation fields because of its advantages of low cost, high safety, environmental protection, and less loss [1–3]. Oil and natural gas pipelines are made of metal material. Due to internal and external factors such as their weight, internal and external loads, material aging, external environment, and pipeline structure displacement, stress concentration can easily occur, leading to major safety accidents such as pipeline rupture, leakage, and explosions [4–9]. Therefore, identifying pipeline stress concentration states and taking corresponding solutions to prevent safety accidents effectively is of great significance to ensuring energy security, people's lives, and property safety. The above measures can also promote sustainable economic development and ensure the safe and stable operation of oil and gas pipelines [10].

The in-pipeline inspection technology is the most economical and effective method to ensure the safety of the pipeline, which takes the transmission medium of the pipeline as the moving force to directly detect the pipeline. At present, the internal inspection technologies of oil and gas pipelines used are mainly Barkhausen stress detection technology, ultrasonic internal inspection technology, far-field eddy current internal inspection technology, and pipeline magnetic flux leakage internal inspection technology [11–13]. The above internal detection methods have been successfully applied in practical engineering, but are mainly used to detect macro defects such as corrosion and cracks. Alternating current stress measurement (ACSM) is a new stress evaluation technology, which has the advantages of fast measurement speed, high sensitivity, and non-contact measurement. It is suitable for internal stress detection of long-distance oil pipelines. For other non-destructive testing technologies, ACSM stress measurement technology overcomes the shortcomings of the Barkhausen measurement signal that is greatly affected by the grain size of the workpiece itself and the microscopic mechanisms of stress and magnetic domain are not yet clear [14]. It has a low cost and high detection efficiency and abandons the requirements of ultrasonic technology for coupling agents [15]. Although the far-field eddy current measurement technology has a large detection depth, its measurement results are greatly affected by lift-off [16]. On the other hand, the change of pipeline magnetic properties may affect the implementation of other subsequent detection methods. Compared with the magnetic flux leakage measurement technology, the ACSM stress measurement technology does not change the magnetic characteristics of the workpiece without magnetization in the measurement process.

Alternating current stress measurement (ACSM) is a non-contact electromagnetic measurement method for stress measurement developed on Alternating Current Field Measurement (ACFM) technology. This method can measure the residual stress dynamically in real-time, with high measurement accuracy, fast measurement speed, and a low requirement on workpiece surface conditions. It is very suitable for the residual stress measurement of long-distance oil and gas transmission pipelines, large measurement areas, and certain requirements on measurement speed [17]. In addition, the method can monitor the residual stress of oil and gas pipelines for a long time. J. Zhou and K. Chen [18,19] studied the influence of stress on the magnetic effect of materials and searched for the internal law of magnetic anisotropy of materials, and the effect of stress on the magnetization of materials. They established the electromagnetic stress model of the material magnetic field changed under stress applications and proposed the ACSM method for the first time. K. Chen [20] further carried out a four-point bending test and tensile test to study the comparison of stress measurement effects under different parameters and combined the previous mathematical model with the stress–magnetization relationship to find the best parameters for stress measurement. Kai Song et al. [21] proposed a stress evaluation method using the ACSM method to quickly judge the direction of principal stress by studying the stress measurement results under the change of the angle α between the direction of the probe excitation magnetic field and the direction of principal stress, which further proved the feasibility of ac electromagnetic field stress measurement technology. W. D. Dover [22] and W. Ricken [23] improved the sensor. The former designed a new type of ACSM stress measurement probe, which improved the measurement sensitivity by using orthogonal excitation. The latter designed a multi-sensor system to reduce the stress measurement error and improve the measurement accuracy. M. J. Knight [20] studied the signal characteristics of ACSM detection of cold-rolled drill collar thread and analyzed the influence mechanism of stress on defects combined with the test results. Songwei Zhou [24] optimized the signal conditioning circuit based on previous studies. He designed two types of single "U" type and orthogonal "U" type probes and analyzed the detection signal characteristics of low carbon steel under a unidirectional tensile and three-point bending loading modes. In addition, he studied the influence of different excitation frequencies and probe angles on detection signals. However, there was no practical engineering application case based on this technology. Therefore, it was of great significance to successfully apply the ACSM detection technology to the internal stress detection of long oil pipelines.

With the large-scale development of oil and gas pipelines, the demand for internal stress detection of long-distance oil pipelines is urgent. Given the above problems, this paper took the application of internal stress detection of long-distance oil pipelines as the background. This paper took the stress test block of oil and gas pipelines as the research object and established a 3D electromagnetic field simulation model for the stress detection of oil pipelines. The magnetic field intensity distribution of the oil pipeline test block (containing the stress area) was analyzed. The diameter-height ratio parameter of the excitation coil was optimized. The influence of different internal and external diameter differences, equivalent radiuses, and heights of the detection coil on the detection sensitivity were compared. The optimal placement position of the detection coil was determined. The ACSM probe was developed. The stress measurement system for internal stress detection of the long-distance oil pipeline was designed and developed. The above system was used for the static tensile test. The influence of excitation frequency and lift-off effect on stress measurement was analyzed. The ability of the system to measure the pipeline stress was verified by measuring the artificial stress area in the actual field traction test, which provided an engineering application foundation and technical support for the internal stress detection of long-distance oil pipelines.

2. Principle of Alternating Current Stress Measurement

When the external magnetic field acts on the ferromagnetic material, its shape, such as length and volume, will change to some extent, which is called magnetostriction. Similarly, when the stress is applied to the ferromagnetic material, the change in its shape can also cause a change in its magnetic properties, namely the inverse magnetostrictive effect, also known as the compressive magnetic effect. The magnetic field will affect the magnetic domain state of the material, making the magnetic domain torque deviate to the direction of the external magnetic field, thus increasing the magnetic field strength in the direction of the external magnetic field. Figure 1 shows the influence of stress and magnetic field on the magnetic properties of materials. As can be seen from the figure, when the pipe is free from stress, its magnetization is zero externally, and a uniform eddy current field is induced on the surface of the pipe. When the local stress concentration occurs in the pipeline due to the external environment and other factors, the change in the local stress state will lead to a change in the permeability of the region. The change of magnetization leads to the distortion of the magnetic force line in the region and generates the disturbed eddy current field. The ACSM probe can characterize the stress by picking up the distorted magnetic field information in the abnormal region.

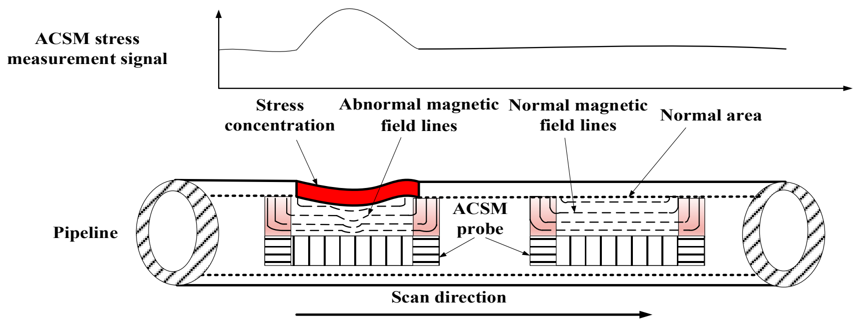

Figure 1. Effects of stress and magnetic field on magnetic domains of ferromagnetic materials.

The ferromagnetic material is placed in a magnetic field with a magnetic field intensity of H, and the magnetic induction intensity is B_1. When no external stress is exerted, the magnetic permeability is $\mu_1 = B_1/H$, and the magnetic energy of the ferromagnetic material is:

$$W_1 = \frac{B_1 H}{2} \tag{1}$$

When an external force is applied to the ferromagnetic material, the magnetic properties of the ferromagnetic material will change. Suppose that the magnetic induction intensity of the ferromagnetic material is B_2, and the permeability is $\mu_2 = B_2/H$, then the magnetic energy of the ferromagnetic material becomes:

$$W_2 = \frac{B_2 H}{2} \tag{2}$$

In a certain magnetic field intensity, the energy change of ferromagnetic material before and after stress is:

$$\Delta W_1 = W_2 - W_1 = \frac{(B_2 - B_1)H}{2} \tag{3}$$

Its pressure magnetic energy changes to:

$$\Delta W_2 = -\sigma\frac{\Delta l}{l} = -\sigma\lambda \tag{4}$$

where σ is the external stress applied, Δl is the deformation caused by the external force of ferromagnetic material, and λ is the material expansion coefficient under the compression-magnetic effect. According to the principle of conservation of energy, before and after stress, the change of magnetization work of ferromagnetic material is equal to the change of magnetic energy caused by stress, namely, $\Delta W_1 = \Delta W_2$, after finishing:

$$\frac{(B_2 - B_1)H}{2} = -\sigma\frac{\Delta l}{l} = -\sigma\lambda \tag{5}$$

Equation (5) is simplified to obtain:

$$(\mu_2 H - \mu_1 H)H = -2\sigma\lambda \tag{6}$$

$$\Delta\mu H^2 = -2\sigma\lambda \tag{7}$$

$$\Delta\mu\left(\frac{B}{\mu}\right)^2 = -2\sigma\lambda \tag{8}$$

When the magnetization of ferromagnetic material under external stress reaches a magnetic saturation state, its magnetostrictive coefficient becomes:

$$\lambda = \lambda_m\frac{B^2}{B_m^2} \tag{9}$$

where λ_m is the saturation magnetostrictive coefficient and B_m is saturation magnetic induction intensity. Substitute Equation (9) into Equation (8) to obtain:

$$\frac{\Delta\mu}{\mu^2}B^2 = -2\sigma\lambda_m\frac{B^2}{B_m^2} \tag{10}$$

$$\Delta\mu = \frac{-2\sigma\lambda_m}{B_m^2}\mu^2 \tag{11}$$

It can be seen from the above formula that the variation of magnetic permeability of ferromagnetic material under the action of a certain external magnetic field is only related to and directly proportional to the external stress of ferromagnetic material. The change of magnetic permeability will cause the change of magnetization intensity in this direction, thus causing the change of magnetic induction intensity in this direction. ACSM stress measurement technology is based on this principle. The ACSM probe picks up the permeability change information caused by stress, which characterizes the stress concentration state.

From the above, the principle of ACSM measurement technology used in this paper is used to pick up the change of permeability caused by stress, so the technology can only be used to measure the stress state of ferromagnetic materials in theory. The material measured in this paper is X52 steel, namely pipeline steel. The material properties of X42–X80 pipeline steel are the same as X52. The different numbers only represent the different yield strength. Therefore, our sensors can still detect the change of their permeability, and then characterize the change of their stress values. Therefore, this technology is feasible for the stress detection of X42–X80 pipeline steel and general ferromagnetic materials.

3. Modeling and Simulation

3.1. Three-Dimensional Electromagnetic Field Simulation Model of an Oil Pipeline

ANSYS finite element analysis software was used to establish the three-dimensional electromagnetic field simulation model of an oil pipeline. The overall three-dimensional solid model was shown in Figure 2, which was mainly composed of an ACSM probe, pipeline plate, and air. Figures 3–5 showed the size and mesh details of the 3D simulation model. In the measurement of pipeline stress, the influence of pipeline wall thickness needs to meet the prerequisite. When the pipeline stress is caused by the external environment of the pipeline, the wall thickness of the pipeline will affect the transmission of external applied force. Whether the wall is thin or thick, the detection effect of this technology is the same when the stress value imposed on the inner wall of the pipeline by external environmental factors is the same. In the range of penetration depth reached by the sensor, the measurement of constant stress value is not affected by the wall thickness.

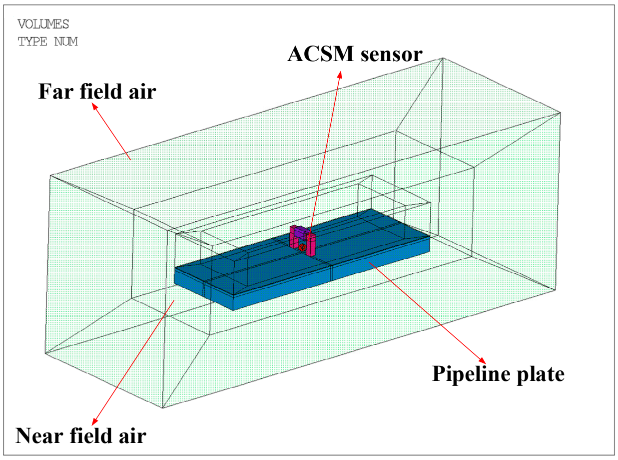

Figure 2. Overall 3D simulation model.

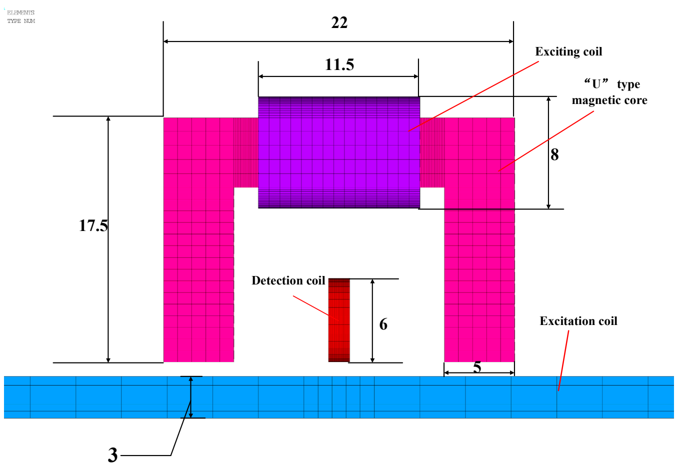

Figure 3. Three-dimensional simulation model size diagram.

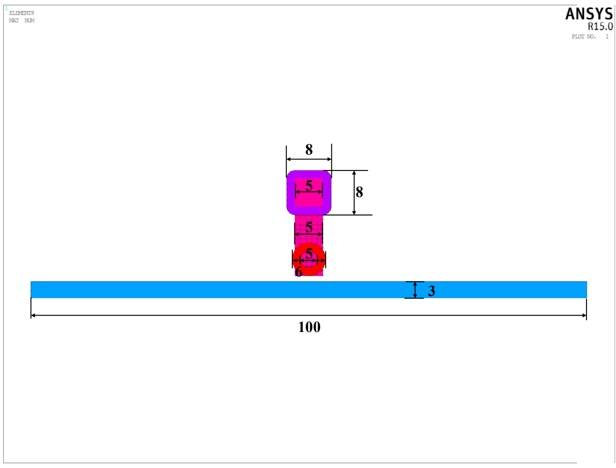

Figure 4. Side view of 3D simulation model.

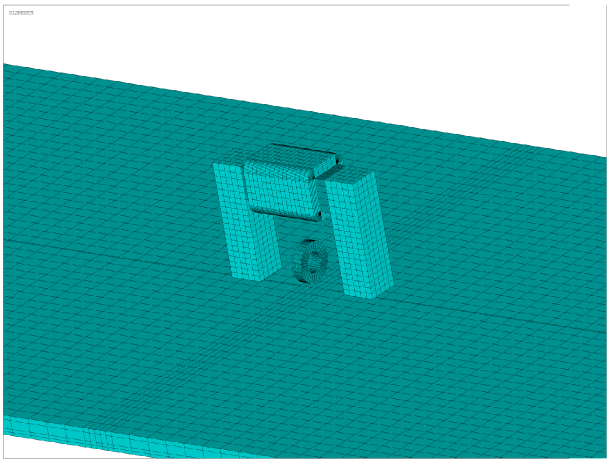

Figure 5. Three-dimensional simulation model grid division details.

In the actual pipeline detection, the pipeline curvature is small, and the volume of the detection probe is smaller. So, in the actual measurement process, our sensor is similar to the measurement on the plate surface, and is basically not affected by the curvature of the pipeline. To reduce the complexity of the model solution and improve the efficiency of the model solution, the pipeline model is replaced by the plate model in the process of model establishment. The specific parameters of the simulation model were shown in Table 1.

Table 1. Simulation calculation model parameters.

Pipeline plate		X52, length = 200 mm, width = 70 mm, thickness = 13 mm, Maximum relative permeability $\mu_r = 670$ (nonlinear and isotropic), and conductivity of material $\sigma = 36\text{Ms/m}$
Excitation coil	AC	Frequency = 4 kHz, 8 Vpp, 300 turns, length = 13 mm, Width = 5 mm, thickness = 5 mm, wall thickness = 1.5 mm, and conductivity of material $\rho = 58.8\text{Ms/m}$
Detection coil		200 turns, inside diameter of 1.5 mm, outside diameter of 3 mm, and conductivity of material $\rho = 58.8\text{Ms/m}$
U-type magnetic core		Arm length = 30 mm, arm height = 5 mm, foot length = 5 mm, foot width = 5 mm, and foot height = 12 mm
Lift-off		1 mm

The key to stress measurement by the ACSM method is the uniform eddy current field located at the center of the U-shaped core. Figure 6 is the magnetic field intensity distribution program on the pipe surface. The two legs of the U-shaped core are located on the surface of the pipe, which induces a vortex current in the opposite direction and finally converges to the central area of the two legs. A uniform eddy current field is formed between the yoke legs. The magnetic field on the pipe surface is symmetrically distributed, and the uniform magnetic field is formed in the central area. Through the simulation results, it can be concluded that the simulation model conforms to the induction law of AC electromagnetic fields and meets the measurement requirements of the ACSM method.

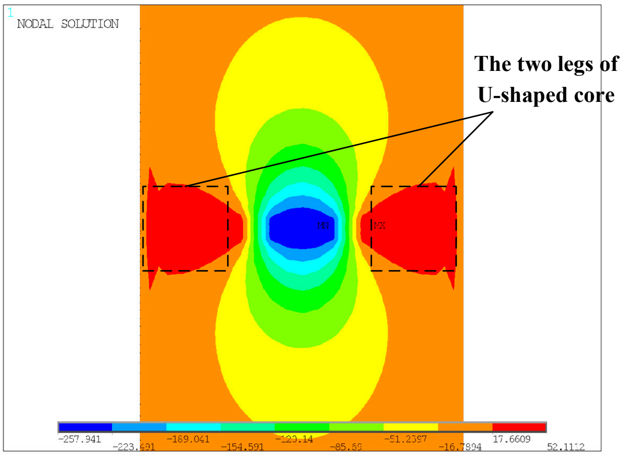

Figure 6. Cloud diagram of magnetic field intensity distribution on the pipe surface.

3.2. Optimization of Excitation Coil Shape Coefficient

When ferromagnetic materials are subjected to external forces, their permeability will change, and there is an approximately linear relationship between the permeability and stress. The ACSM probe can pick up the permeability change information caused by stress, and the information characterizes the stress concentration state. In this section, the change of permeability of the pipeline was used to simulate the real stress change, and the voltage output of the ACSM probe was taken as the analysis object to compare the output voltage change of the probe with different parameters under a certain permeability change. The initial permeability of the pipeline μ_0 (simulated stress not applied) was set to 600, and the change step was set to 5%. Then, the changed permeability μ_n was:

$$\mu_n = \mu_0(1 + \Delta\mu_n) \tag{12}$$

The 3D excitation coil model established in the simulation was shown in Figure 7, where D was the thickness of the excitation coil and L was the length of the excitation coil wound on the magnetic arm of the U-shaped magnetic core. Ψ was defined as the ratio of the thickness of the excitation coil, D, to the length of the excitation coil, L, denoted as:

$$\Psi = D/L \tag{13}$$

The excitation frequency was set to 4 kHz, the excitation voltage was set to 8 Vpp, and the number of turns of the excitation coil was set to 180. Keeping other parameters unchanged, the change of the output voltage difference of the ACSM probe with the shape coefficient of the excitation coil, Ψ, is shown in Figure 8. It could be found that when the change in permeability, $\Delta\mu_n$, was 125%, the output voltage difference decreased approximately linearly with the increase of lift-off height. The influence of the excitation coil shape coefficient on the measured signal was monotonic, when the excitation coil shape coefficient was 0.115, 0.277, 0.318, 0.640, and 0.785. The induced voltage differences of the probe were 1.276×10^{-2} V, 0.829×10^{-2} V, 0.66×10^{-2} V, 0.505×10^{-2} V, and

0.437×10^{-2} V, respectively. The induced voltage difference of the probe decreases with the increase of the shape coefficient, decreasing by about 65.75%. It can be seen that when winding the excitation coil, the probe measuring the sensitivity of the "chunky" winding mode was higher than the "thin and high" winding mode. It meant the excitation coil with a large diameter-to-height ratio had a better detection effect.

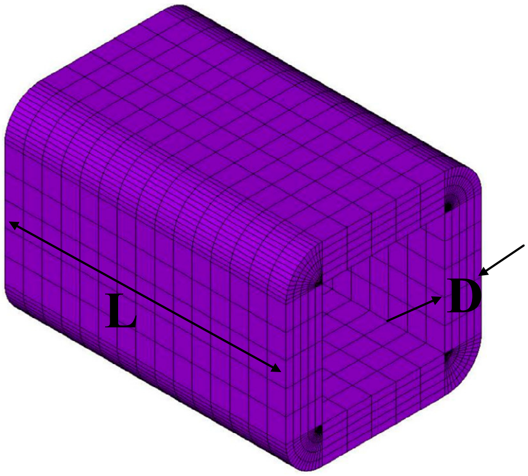

Figure 7. Three-dimensional simulation model of the excitation coil.

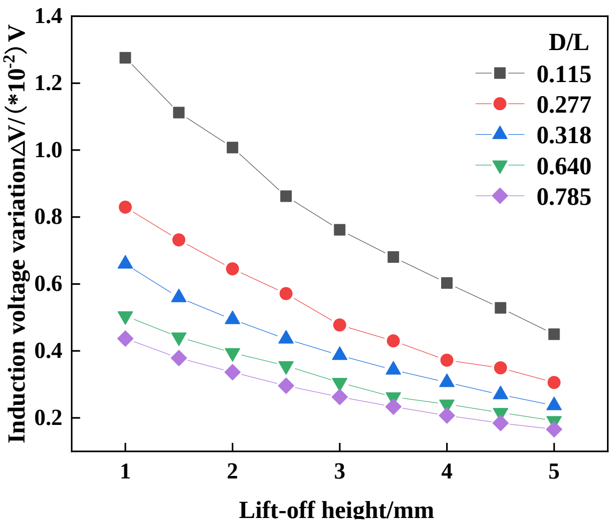

Figure 8. The shape coefficient of excitation coil affects the curve.

3.3. Detection Coil Optimization

The design of the detection coil was based on Faraday's law of electromagnetic induction. When the probe passed through the stress concentration area of the pipeline, the abrupt and distorted magnetic field signal was generated, and the magnetic flux coupled to the detection coil changed. So, the induced electrodynamic force would be generated. Figure 9 showed the 3D simulation model of the detection coil established in the simulation. The height of the detection coil was h. The inner diameter was r_1 and the outer diameter was r_2. To better study the stress measurement performance of probes with different parameters, the average radius, $\bar{r} = (r_1 + r_2)/2$, was defined, $\Delta r = (r_2 - r_1)$, as the difference between the inner and outer diameters of the detection coil, and the influence of the difference between the inner and outer diameters of the detection coil on the stress measurement performance of the probe was studied:

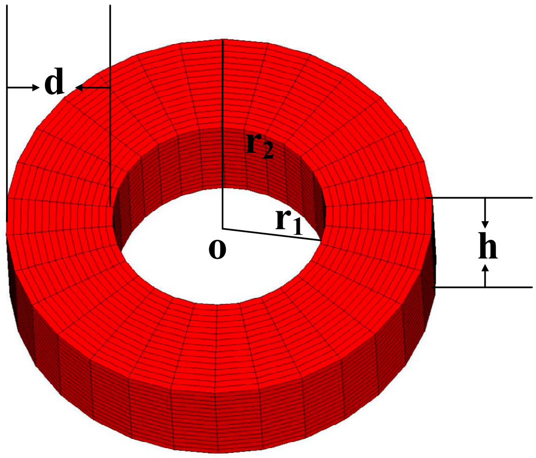

Figure 9. Detection coil 3D simulation model.

The average radius, $\bar{r}$, and height, h, of the ACSM probe detection coil were set as 2.25 mm and 1.5 mm. The average radius, $\bar{r}$, and height, h, of the probe detection coil were unchanged. The inner and outer diameter difference, Δr, was set to 0.5 mm, 1.5 mm, and 2.5 mm. When the $\Delta\mu_n$ was 125%, the difference of the probe output voltage with different inner and outer diameter difference parameters changes with lift-off, as shown in Figure 10.

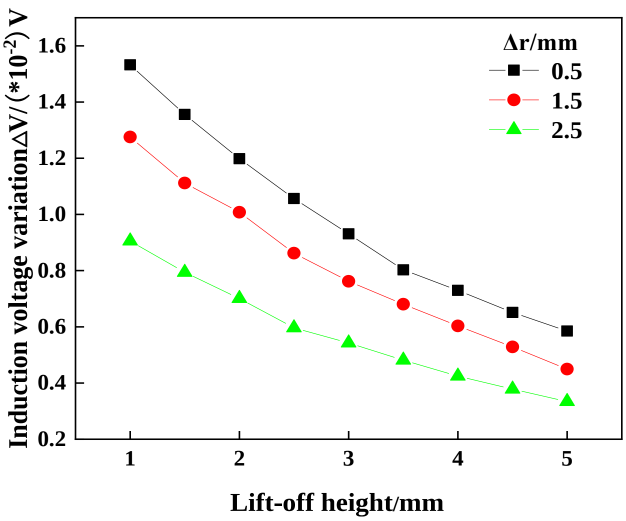

Figure 10. The influence of inner and outer diameter difference of the detecting coil on measuring signal.

As shown in Figure 10, with the inner and outer diameter difference of the probe test coil increasing, the differential voltage from the sensor under any lift-off was decreased. The induction voltage difference decreased more and more gently with the increase of the probe lift-off height. The chart was divided into two parts, 1–3 mm lift-off height was the first part, 3–5 mm lift-off height was the other part. The average slope of the curves in these two parts, $\bar{k}$ was used to characterize the downward trend. The average slope under different diameter differences, $\bar{k}$, changed as shown in Table 2. It could be seen that the average slope of $\bar{k}$ decreased with the increase of the inner and outer diameter difference of Δr of the probe detection coil. It indicated the small inner and outer diameter difference of Δr of the probe detection coil was beneficial for improving the average slope and induced voltage of the output voltage of the probe. At this point, the probe had a higher measurement sensitivity.

Table 2. The average slope of the measured signal when the coil is detected with different inner and outer diameters difference.

Inner and Outer Diameter Difference Δr/mm	Lift-Off the Average Slope $\bar{k}$ in the Range of 1–3 mm	Lift-Off the Average Slope $\bar{k}$ in the Range of 3–5 mm
0.5	−3.005	−1.730
1.5	−2.570	−1.560
2.5	−1.810	−1.040

3.4. Optimization of the Excitation Coil and Detection Coil Relative Position

It can be seen from Equation (12) that μ_n was the permeability after the change and $\Delta\mu_n$ was the percentage change of permeability. The permeability change step was set to 5%, ranging from 0 to 125%. There were 26 groups $(\mu_0 - \mu_{25})$ in total. The excitation frequency was set to 4 kHz and the excitation voltage was set to 8 Vpp. In this section, the influence of the relative position of the excitation coil and the detection coil on the measurement signal under 1 mm of lift-off was explored through the simulation. Figure 11 was the 3D simulation model of the ACSM probe established in the simulation, which was mainly divided into the excitation part and the detection part. The excitation part consisted of a U-shaped magnetic core and an excitation coil wound on the arm of the magnetic core. The detection part mainly referred to the detection coil located just below the center of the excitation coil.

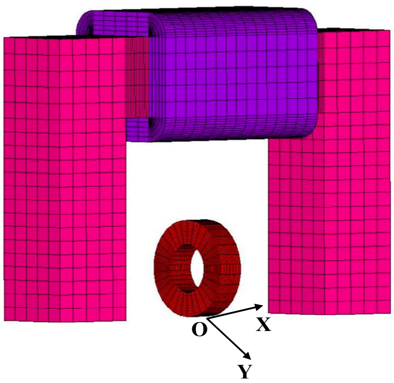

Figure 11. ACSM probe 3D simulation model.

As shown in Figure 12, the excitation part was kept fixed, and the detection coil was shifted 4 mm from the positive center (point O in the figure) to the X direction (the direction of bipedal connection) and Y direction (the vertical direction of bipedal connection), respectively. Data were extracted and saved every 1 mm, and the voltage difference was obtained after differential processing:

$$\Delta V_n = V_n - V_0 \tag{14}$$

Among them, ΔV_n was the probe output voltage after the difference. V_n was the output voltage of the probe when the pipeline permeability was μ_n. V_0 was the output voltage of the probe when the pipeline permeability was μ_0. The results after data differences were shown in Figure 13a,b. When μ_n = 125%, the curve of the probe output voltage difference changed with the detection coil offset distance as shown in Figure 13c.

Figure 10 showed that the output voltage of the ACSM probe changed approximately linearly with the change in permeability. When the detection coil was located at the center of the connection between the two pins of the U-shaped magnetic core, the probe measurement sensitivity was the highest. When the detection coil was offset in the X direction or the Y direction, the probe measurement sensitivity would decrease. As can be seen from Figure 13c, when the detection coil was offset in the X direction and the Y direction by 4 mm, the output-induced voltage difference of the probe was 1.141×10^{-2} and 1.163×10^{-2}, which were reduced by 10.58 and 8.86%. Therefore, when the detection coil was located at the center of the two pins of the U-shaped core, the probe measurement sensitivity reached the maximum.

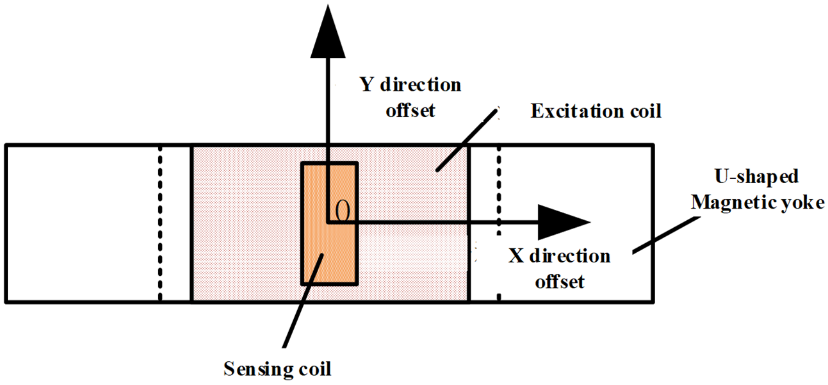

Figure 12. Schematic diagram of detecting the coil offset.

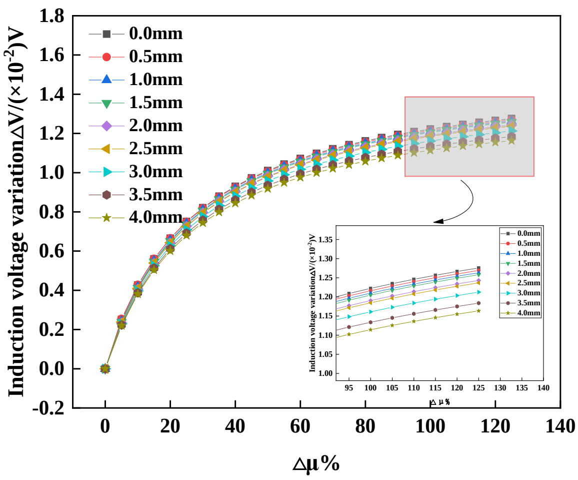

(**a**)

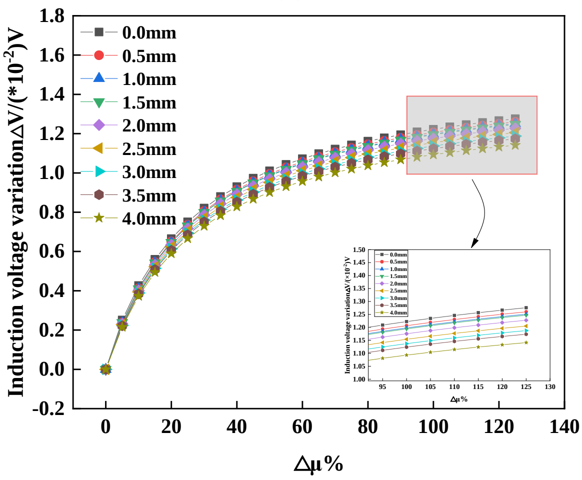

(**b**)

Figure 13. *Cont.*

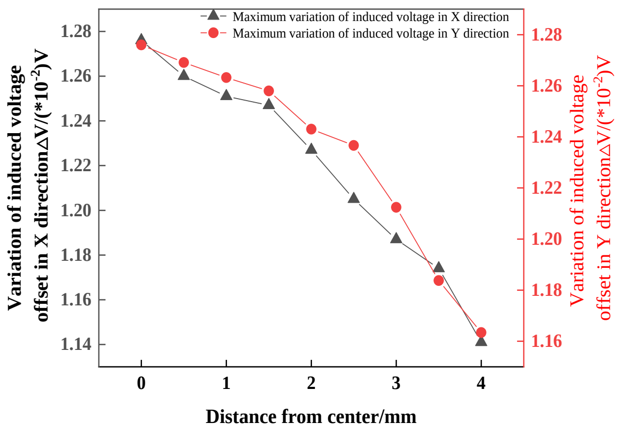

(c)

Figure 13. Influence of excitation coil/detection coil relative position on signal. (**a**) The induced voltage varies with permeability when the X direction is offset. (**b**) The induced voltage varies with permeability when the Y direction is offset. (**c**) Detection coil offset distance change influence curve.

4. System Construction and Experimental Optimization

4.1. Construction of the ACSM Stress Measurement System

The overall structure block diagram of the oil pipeline stress measurement system based on the ACSM method is shown in Figure 14. The measurement system mainly includes a power supply module, signal excitation module, stress measurement probe, signal conditioning module, AD conversion module, data storage module, and upper computer display module.

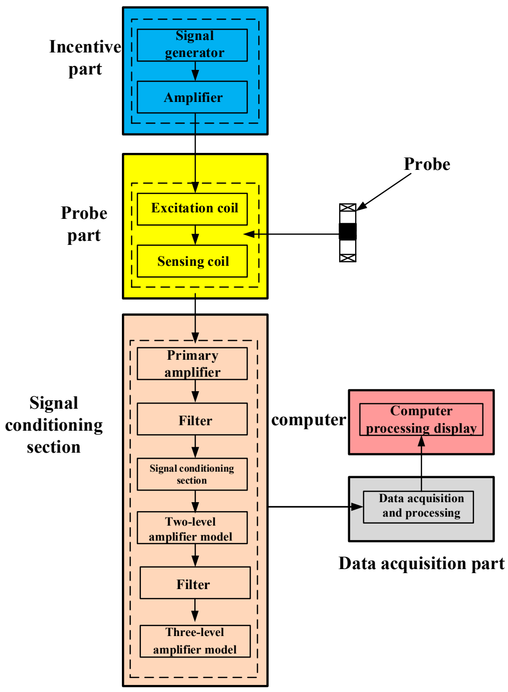

Figure 14. Structural block diagram of the internal stress measurement system for an oil pipeline.

The specific workflow for a stress measurement system comprises: power supply module for the measuring system, required for each module and providing a stable dc voltage. The signal generator module produced two sine signals. A sinusoidal signal as an excitation signal provided a uniformly varying magnetic field to the surface of the pipe. The other sinusoidal signal as a reference signal was input to the signal conditioning module. The ACSM stress measurement probe is shown in Figure 15. The excitation part is composed of a rectangular excitation coil and U-shaped magnetic core, which is mainly used to generate a uniform magnetic field on the workpiece surface. The magnetic signals containing stress information are picked up by the ACSM probe and converted into electrical signals, which are successively sent to the amplification circuit module, signal conditioning module, two-stage amplification module, and A/D conversion circuit module. After the conversion, the magnetic signals are sent to the upper computer for real-time curve display and stored in the memory module.

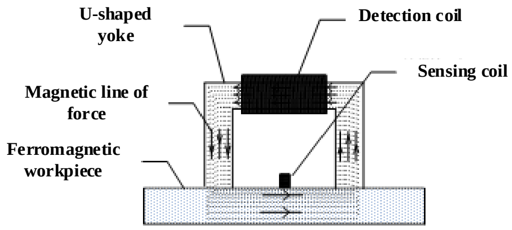

Figure 15. ACSM sensor.

The upper machine system design mainly includes the front panel and rear panel program block diagram. The front panel functions mainly to realize the real-time display of stress measurement signals and set the relevant measurement parameters of each function module. The rear panel mainly realizes the specific functions of the stress measurement curve real-time display, parameter setting, signal processing, threshold alarm, and other functional modules by using graphical programming. The structural block diagram of the overall design of the system software is shown in Figure 16.

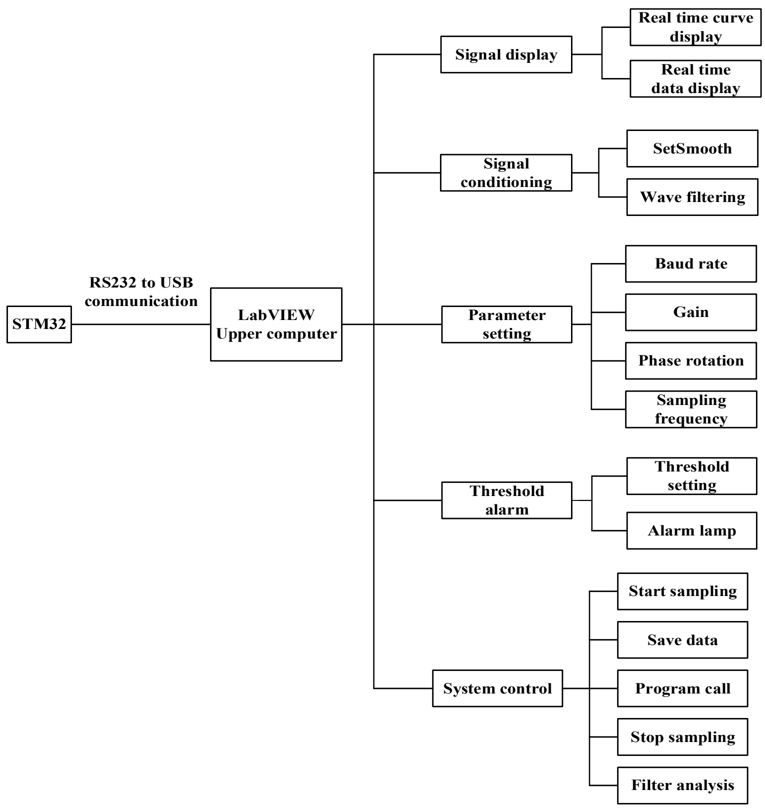

Figure 16. System software overall design structure block diagram.

LabVIEW was a product of the National Instruments Corporation of the United States. Its inventor was Jeff Kodosky. The upper computer software interface was compiled by

LabVIEW2014, which mainly includes five parts: signal display, signal conditioning, parameter setting, threshold alarm, and system control module. As shown in Figure 17, the signal display module mainly realized the real-time display of stress measurement curves and measurement data. Through the combination of curves and data, stress measurement signals could be analyzed more intuitively and quickly. The signal processing module mainly realized smoothing, digital filtering, and amplification of the collected stress measurement signal to filter the interference noise and improve the signal-to-noise ratio. The parameter-setting module mainly realized the setting of the relevant measurement parameters. It realized the display and adjustment of the measurement signal by setting the relevant measurement parameters such as baud rate, grain size, phase, and sampling frequency. The threshold alarm module mainly realized threshold setting and threshold alarm function. The system control module mainly realized the system program running, stopping, reset, waveform analysis, program call, and other related functions.

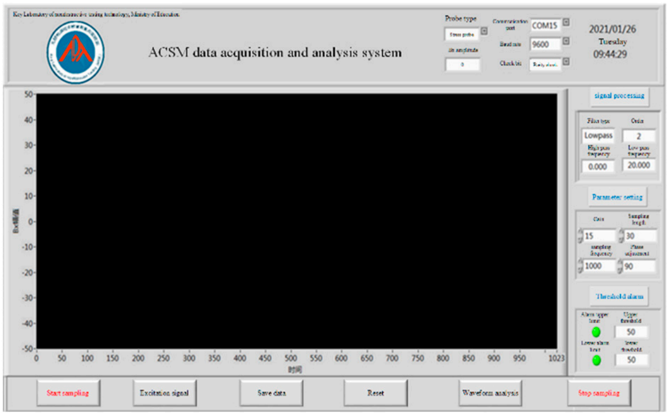

Figure 17. The host computer interface of ACSM stress measurement system.

The ACSM stress measurement system developed in this paper was used to carry out subsequent experimental studies. The ACSM stress measurement system was mainly composed of three parts: computer, instrument box, and ACSM stress measurement probe. The physical picture of the system is shown in Figure 18. After the test of the ACSM stress measurement system, to improve the portability of the system and facilitate the carrying of other external systems, the ACSM stress measurement board was specially developed, which was highly integrated and had a high degree of customization. It could be applied to the inner wall detection of oil and gas pipelines. The self-adaptive pipeline crawler could realize the full circumferential real-time dynamic measurement of the inner wall of oil and gas pipelines. The ACSM stress measurement board card is shown in Figure 19.

Figure 18. ACSM stress measuring instrument physical drawing.

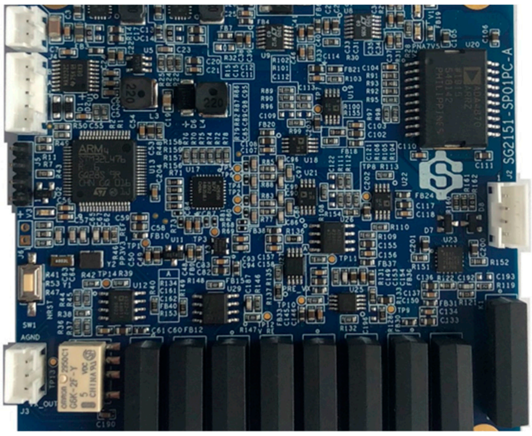

Figure 19. ACSM stress measurement board.

4.2. Test and Verification

4.2.1. Study on the Static Tensile Test

The static load tensile testing machine was used to draw the test block uniformly until it broke. The actual yield strength of the test block was about 35 kN (350 MPa). The developed ACSM stress measurement system was used to measure the static load tensile stress of the X52 profile steel test block under different measuring parameters, as shown in Figure 20. The stretching range was set as 0–30 kN (0–300 Mpa), the stretching speed of the test block was 0.5 mm/min, and the output voltage value of the sensor, V_n, was recorded at 1 kN intervals. The initial voltage value of the sensor without stretching was denoted as V_0, and the change curve of the output voltage value of the sensor $(V_n - V_0)$ with stress was obtained.

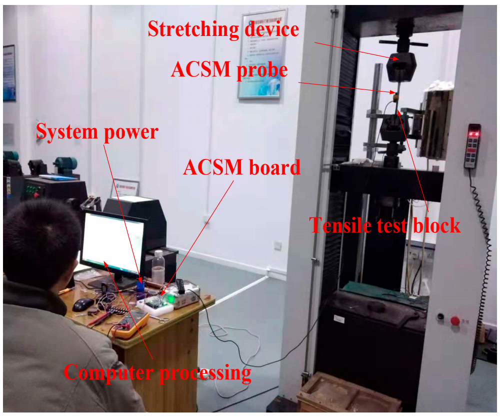

Figure 20. Assembly drawing of the static tensile test block.

The excitation frequency was set to 4 kHz, peak-to-peak value of excitation voltage was 8, and the number of excitation turns was set to 160. Only the excitation frequency range was changed to 3–7 kHz. The amplitude of the Bx characteristic quantity was taken as the stress evaluation index, and the change curve between the measured signal change and stress is shown in Figure 21.

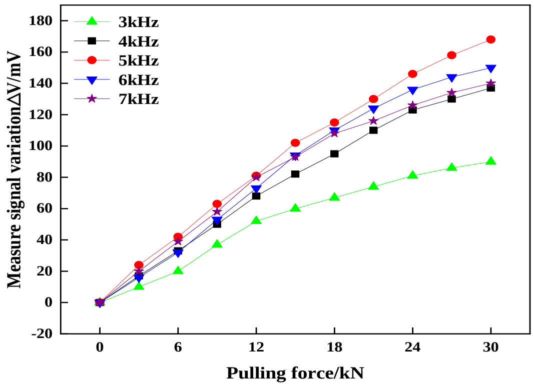

Figure 21. The curve of measuring signal of the probe with tension.

4.2.2. Excitation Frequency Optimization with Tension Curve

The excitation frequency was affected by the skin effect. In the process of stress measurement, the sensitivity of the probe was different at different frequencies. Therefore, it was necessary to select the best excitation frequency suitable for stress measurement.

It can be seen from Figure 22a that with the increase of excitation frequency, the change of the measured signal generally increased first and then decreased, and the change of the measured signal reached the maximum when frequency F was 5 kHz. Further analysis is shown in Figure 22b. Within the range of excitation frequency of 3–5 kHz, the change amount of the measured signal, measurement sensitivity, linear correlation coefficient, and change rate of the measured signal had the same change trend with the increase of excitation frequency. They showed a trend of first increasing and then decreasing. Within the range of an excitation frequency of 3–5 kHz, the variation of the measured signal increased with the increase of excitation frequency. When the excitation frequency F was 3 kHz, the minimum measured signal change was 90 mV; when the excitation frequency F was 5 kHz, the maximum measured signal change was 168 mV; when the excitation frequency was 5–7 kHz, the measured signal change decreased with the increase of the excitation frequency. When the excitation frequency F was 6 to 7 kHz, the measured signal changes were 150 mV and 140 mV, respectively, which decreased by 10.71% and 16.67%, and the sensitivity decreased by 5.55 and 15.89%. Compared with when the frequency F was 5 kHz, the linear correlation coefficient R^2 decreased by 10.42 and 27.01%, and the change rate decreased by 17.83% and 28.4%, respectively. Therefore, the excitation frequency F = 5 kHz was a turning point of the measurement parameters, and the optimal excitation frequency for stress measurement was 5 kHz.

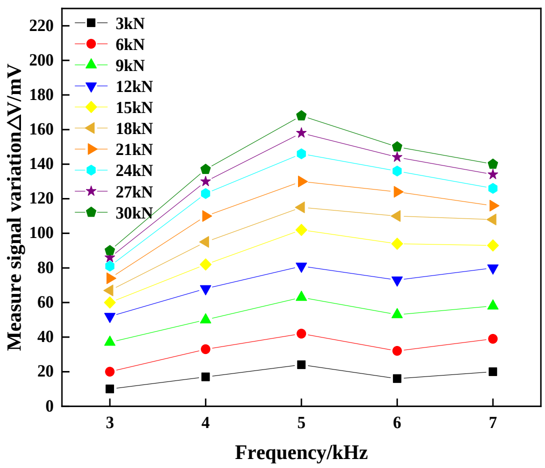

(**a**)

Figure 22. *Cont.*

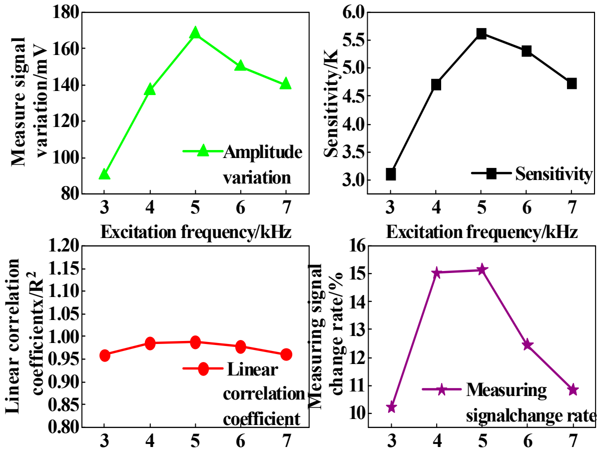

(**b**)

Figure 22. Influence of excitation frequency on the stress measurement signal. (**a**) Variation curve of probe measurement signal with a frequency. (**b**) Influence of excitation frequency on each characteristic quantity.

4.3. Pull Test

The developed stress measuring board was used to measure the stress of the oil pipeline by the ACSM method. The engineering demonstration test had an important reference significance for the study of internal stress measurement of an oil pipeline through the on-site pull test of internal stress measurement of the oil pipeline. As shown in Figures 23 and 24, the pull test described in this section was carried out in actual oil pipelines. The ACSM stress measurement probe and the ACSM stress measurement system card used in this experiment were embedded in the pipeline crawler to realize the automatic measurement of the internal stress of the pipeline. As shown in Figure 25, in order to reduce the influence of pipeline noise and girth weld area in the measurement process, two groups of experiments were used to eliminate the noise signal of common signal characteristics. When the noise signal is excluded, the obvious mutation signal feature is the stress signal. There were two ACSM probes, which were respectively placed at the position of 12 o'clock and 6 o'clock in the circumferential direction of the pipeline, and the pulling speed was 5 m/s. During the test, the stress measurement data were stored in real-time using the built-in memory of the system.

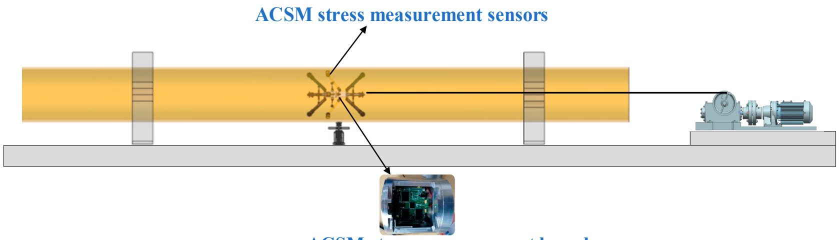

Figure 23. Assembly diagram of the stress measuring instrument.

The test was divided into two times: one was with no human intervention for the first-time pull experiment. The second position was set as the positioning section in the fifth section of the pipeline, and the jack was placed at the bottom of the positioning section at six o'clock to lift the pipeline. The constant test parameters were ensured to compare the two stress measurement results of the pipeline positioning section, as shown in Figure 26.

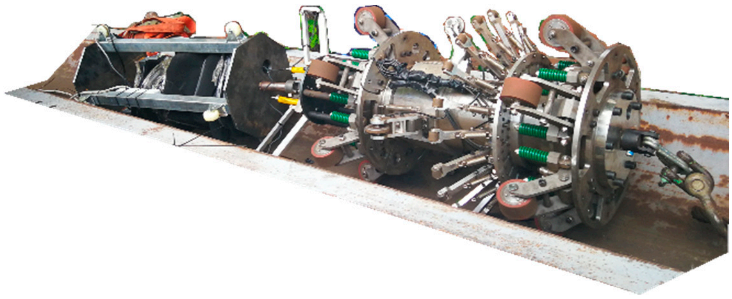

Figure 24. The working picture of the stress measuring instrument.

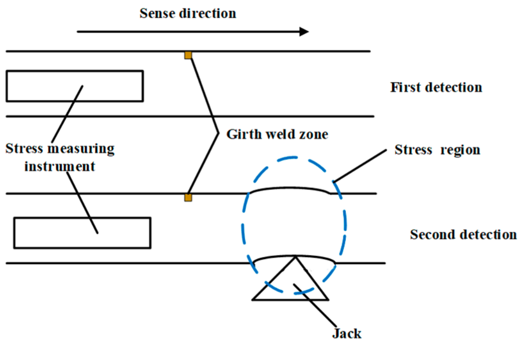

Figure 25. Principle diagram of the traction test.

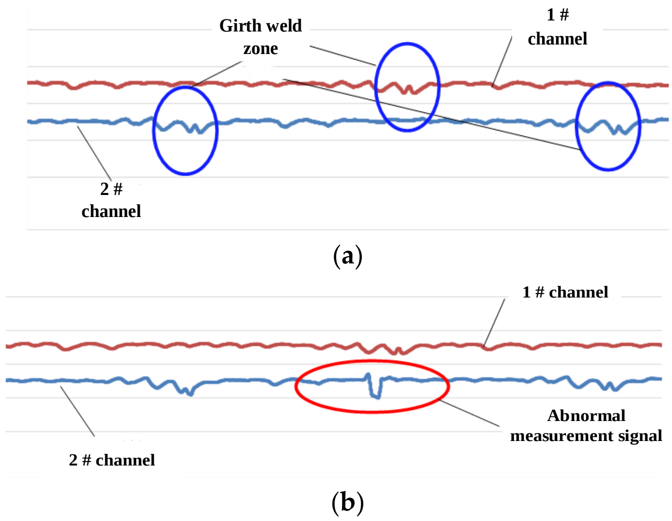

Figure 26. Tension test stress measurement results. (**a**) Stress measurement results of locating the section of the inner wall without manual intervention. (**b**) Stress measurement results from locating the section of the inner wall during manual intervention.

Figure 26a showed that without human intervention, the pipeline stress measurement signal characteristics were regular. (To facilitate analysis and comparison, only the stress measurement signal of the pipeline positioning section was analyzed.) The 1# and 2# probe placements were different, but the measured stress signal changed regularly. The signal mutations happened in the pipeline girth weld, with small noise signal fluctuations in the other location. The actual pipeline stress testing process is needed to analyze the signals of multi-channel measurement at the same time. The introduction of the "relative change" concept was restricted by site conditions, and multi-channel signals at the same time appear as big or small-signal mutations (possibly caused by the girth weld or rough surface). At this time, it was considered that the "relative signal" did not appear obviously abnormal. When only one of the multi-channel signals appeared inconsistent with most other signals, it was considered that the "relative signal" was abnormal and stress concentration occurred at the position corresponding to this channel.

Figure 26b showed the stress measurement results of the positioning section of the pipeline when manual intervention was applied for the second time. By comparing the two stress measurement results in Figure 21, it was found that probe 2# in the positioning section of the pipeline has an obvious abrupt signal relative to probe 1# when manual intervention was applied. This was because the area measured by the 2# probe at the bottom of the pipeline was exactly the jack lifting area. So, an obvious abrupt signal was generated when it passed through the positioning section of the pipeline. The amplitude of the stress mutation signal reached 240 mV and the amplitude of the large noise signal (the girth weld) was 70 mV. The amplitude of the small noise signal was only 45 mV. The maximum S/N could reach 5:1. By comparing the two data sets, it was proved that the system could identify the stress concentration area of the pipeline effectively.

5. Conclusions

In this paper, an ACSM stress measurement probe and an integrated stress measurement system were proposed. The simulation results showed that the sensitivity of the ACSM stress measurement probe decreased with the increase of the shape coefficient of the excitation coil. Reducing the inner and outer diameter difference of the detection coil could effectively improve the sensitivity of the probe. However, when the inner and outer diameter difference of the detection coil was reduced to a certain extent, the sensitivity improvement effect was not obvious. When the parameters of the excitation coil and the detection coil were fixed, the measurement effect was the best when the detection coil was located at the center of the legs of the U-shaped magnetic core. When the ACSM stress measurement probe was applied to the excitation frequency of 3–5 kHz, the variation of the measured signal, the measurement sensitivity, the linear correlation coefficient, and the change rate of the measured signal had the same trend as the increase of the excitation frequency, which increased first and then decreased. When the excitation frequency was F = 5 kHz, it was the highest sensitivity of the probe. The sensitivity of the probe was inversely proportional to the height of the detection coil. When the coil height increased from 1.5 mm to 2 mm and 3 mm, the signal amplitude change rate decreased by 34.66% and 60.67%, respectively. The engineering practice of ACSM stress detection of the oil pipeline was carried out by using the developed stress measurement system, and the stress measurement results of the inner wall of the two positioning sections were compared and analyzed. There was an obvious abnormal mutation signal in the artificial stress of the pipeline positioning section, indicating that the system could effectively identify the stress concentration area of the pipeline.

The limitation of this technology is that only the stress measurement method of ferromagnetic materials is studied according to the change of material permeability. In addition, due to the measurement principle of ACSM technology, the penetration depth and energy field strength of this technology need to be further improved. For the subsequent development of the technology, the replacement of non-ferromagnetic materials such as aluminum, copper, and other types of composite materials for stress measurement research can be considered to expand the application range of the system. In this paper, the stress measurement experiment of ferromagnetic materials in the elastic region is mainly carried out. The stress measurement of ferromagnetic materials in the inelastic deformation can be further carried out by using this system. In the pipeline engineering stress measurement test, artificial stress was measured in this test. In future work, different types of stress concentration should be expanded, and the stress measurement should be carried out to analyze the signal law.

Author Contributions: Conceptualization, J.D. and K.S.; methodology, J.D. and K.S.; software, J.D. and W.X.; validation, J.D., K.S., G.J. and W.X.; formal analysis, J.D.; investigation, K.S.; resources, G.J.; data curation, J.D., W.X. and C.S.; writing—original draft preparation, J.D. and K.S.; writing—review and editing, J.D. and G.J.; visualization, J.D. and C.S.; supervision, J.D. and K.S.; project administration, K.S.; funding acquisition, K.S. and G.J. All authors have read and agreed to the published version of the manuscript.

Funding: National Natural Science Foundation of China (Project No.: 51865033), Research on Defect Detection and Evaluation Technology of High-grade Steel Pipeline (Project No.: WZXGL202104).

Institutional Review Board Statement: Not applicable.

Informed Consent Statement: Not applicable.

Data Availability Statement: Not applicable.

Conflicts of Interest: The authors declare no conflict of interest.

References

1. Li, C.; Cui, W.J.; Cheng, W.G. Current situation analysis and Structural innovation of oil pipeline Engineering. *Theor. Res. Urban Constr. Electron. Ed.* **2013**.
2. Wang, B.Q.; Lin, Y.H.; Dai, Y.B.; Cai, X.Y. Present situation and prospect of crude oil pipeline in China. *Pet. Plan. Des.* **2012**, *23*, 8–11.
3. Chen, Q.W. A Brief Discussion on Anticorrosion Technology of Petroleum Pipeline Engineering. *New Technol. New Prod. China* **2019**, *22*, 68–69.
4. Chen, L.L. Stress design of petrochemical pipelines. *China Pet. Chem. Stand. Qual.* **2019**, *39*, 124–125.
5. Zhou, C.J. River. Pipeline stress analysis in petrochemical design. *Shandong Chem. Ind.* **2017**, *46*, 129–130.
6. Wang, Y.L. Research on stress design of petrochemical pipelines. *China Chem. Trade* **2019**, *11*, 29.
7. Ma, Y.; Qin, X.M.; Peng, S. Corrosion Causes and Anticorrosion of Petroleum Pipelines. *Chem. Des. Commun.* **2019**, *45*, 30–31.
8. Pang, X.R. Destruction and nondestructive testing of petrochemical pressure pipelines. *Petrochem. Technol.* **2019**, *26*, 218.
9. Zhou, Z.C. Thinking on the Safety of China's oil and gas pipeline network. *China Chem. Trade* **2012**, *11*, 208.
10. Wang, Y.Q. Brittle Failure Tendency of Steel Structural Members in High Stress Concentration Area. *Eng. Mech.* **1995**, *3*, 132–138.
11. Wang, Q.M.; Sun, Y. Progress and Trend of Residual Stress Testing Technology. *Electromech. Eng.* **2011**, *28*, 11–15.
12. Liu, Q.Q.; Liu, Z.S.; Song, S.; Xie, L.L. Review of residual stress measurement. *Mach. Tools Hydraul.* **2011**, *39*, 135–138.
13. Chen, H.L.; Zhong, Y. Research Progress of Residual Stress Testing Methods. *Yunnan Metall.* **2005**, *3*, 52–54.
14. Wang, S.Z.; Ren, X.D.; Qiao, H.Y.; Ge, Z.L. Evaluation of residual stress Barkhausen effect on ferromagnetic material surface. *Nondestruct. Test.* **2013**, *35*, 26–28.
15. Lu, H.; Xing, L.W.; Xing, J.W. Ultrasonic welding residual stress measurement technology. *Welded Pipe* **2019**, *42*, 50–55.
16. Feng, Q.; Li, R.; Nie, B.; Liu, S.; Zhao, L.; Zhang, H. Literature review: Theory and application of online detection technology for girth weld defects of oil and gas pipelines. *Sensors* **2016**, *17*, 50. [CrossRef]
17. Topp, D. Recent Developments and Applications of the ACFM Inspection Method and ACSM Stress Measurement Method. *Non-Destr. Test. Aust.* **2005**, *42*, 141–147.
18. Zhou, J.; Dover, W.D. Electromagnetic induction in anisotropic half-space and electromagnetic stress model. *J. Appl. Phys.* **1998**, *83*, 1694–1701. [CrossRef]
19. Chen, K.; Brennan, F.P.; Dover, W.D. Thin-skin AC field in anisotropic rectangular bar and ACPD stress measurement. *NDT E Int.* **2000**, *33*, 317–323. [CrossRef]
20. Chen, K.; Brennan, F.P. A theoretical and experimental study of alternating current stress measurement under different loading modes. *J. Strain Anal. Eng. Des.* **1998**, *33*, 291–303. [CrossRef]
21. Song, K.; Hou, K.; Wang, C.; Xu, C.; Wang, Z. The stress characterization of ferromagnetic components based on ACSM method. *Mech. Eng. J.* **2018**, *54*, 16–22. [CrossRef]
22. Han, S.; Brennan, F.P.; Dover, W.D. Development of the alternating current stress measurement model for magnetostriction behaviour of mild steel under orthogonal magnetic fields for stress measurement. *J. Strain Anal. Eng. Des.* **2002**, *37*, 21–31. [CrossRef]
23. Ricken, W.; Schoenekess, H.C.; Becker, W.J. Improved multi-sensor for force measurement of pre-stressed steel cables by means of the eddy current technique. *Sens. Actuators Phys.* **2006**, *129*, 80–85. [CrossRef]
24. Song, K.; Zhou, S.W.; Wang, C.; Zhang, L.P. ACSM system design and stress measurement of ferromagnetic components. *J. Sens. Technol.* **2014**, *27*, 267–271.